Journal of Scientific and Human Dimensions
مجلة الأبعاد العلمية والإنسانية
Volume 1, Issue 2, 2025, Pages: 362-373
Journal homepage: https://jshd.com.ly/index.php/jshd/en

Adaptive Weighted Multitaper Method for Spectral Estimation Under Data Loss

Alsanousi Aboujanah[1 *], Ramadan A M Khalifa[2], Giuma Amara Abushafa[3]
[1]Department of Communication Engineering, High Institute of Science and Technology, Tamzaoua Alshati, Alshati, Libya
[2]Department of Communication Engineering, High Institute of Science and Technology, Suk Algumaa, Libya
[3]Department of communication Engineering, Faculty of Engineering, AlMergib University, AlKhoms, Libya

تقدير الطيف مفقود البيانات باستخدام طريقة الأوزان المتعددة التكيفية

السنوسي موسى ابوجناح[1*]، رمضان المبروك خليفة[2]، جمعة اعمارة ابوشعفة[3]
[1]قسم التقنيات الكهربائية والالكترونية، المعهد العالي للعلوم والتقنية تامزاوة الشاطئ، الشاطئ، ليبيا
[2] قسم التقنيات الكهربائية والالكترونية، المعهد العالي للعلوم والتقنية سوق الجمعة طرابلس، طرابلس، ليبيا
[3]قسم هندسة الاتصالات، جامعة المرقب الخمس، الخمس، ليبيا

[*]Corresponding author: sanouci@histtam.edu.ly

Received: October 14, 2025	Accepted: December 20, 2025	Published: December 29, 2025

Abstract:
Modern radar systems frequently encounter data loss during signal acquisition due to hardware failures, interference, or intermittent sampling, severely degrading spectral estimation accuracy. This work introduces an adaptive weighted multitaper method integrated with a circular memory architecture to address spectral leakage under adverse conditions with substantial missing data. Our approach employs a novel weighting scheme were systematically optimized through grid search across 200 parameter combinations using 500 Monte Carlo trials. Testing across SNR levels 0-30 dB with 30% missing data reveals substantial improvements Comparative analysis against the Bartlett, Welch, and Thomson Multitaper methods. For typical radar parameters (N=1024, K=8, M=128), our method requires approximately 8,192 operations versus 40,960 for Thomson MTM, representing a kind of 80% computational reduction while maintaining superior performance. The method proves effective for radar applications requiring robust spectral estimation despite incomplete data acquisition, maintaining computational efficiency suitable for real-time processing.

Keywords: Spectral estimation, Circular memory, Data loss, Power spectrum, Adaptive weighting, Multitaper method, Radar signal processing**.**

الملخص
تواجه أنظمة الرادار الحديثة فقداناً متكرراً للبيانات أثناء عملية اقتناء الإشارة، وذلك بسبب أعطال الأجهزة أو التداخلات الخارجية أو أخذ العينات بشكل متقطع، مما يؤثر بشكل كبير على دقة التقدير الطيفي. يقدم هذا البحث طريقة متعددة الأوزان بترجيح تكيفي، مدمجة مع معمارية ذاكرة دائرية، لمعالجة مشكلة التسرب الطيفي في ظل الظروف القاسية التي تتضمن فقداناً كبيراً في البيانات. يعتمد نهجنا على آلية ترجيح مبتكرة بشكل منهجي من خلال البحث الشبكي عبر 200 تركيبة من المعاملات باستخدام 500 محاكاة مونت كارلو.

أظهرت الاختبارات عبر مستويات نسبة الإشارة إلى الضوضاء من 0 إلى 30 ديسيبل مع فقدان 30% من البيانات تحسينات ملموسة في دقة التردد وكبت الضوضاء، بما يؤكده التحليل المقارن مع طرق بارتليت وويلش وثومسون متعدد الأوزان. بالنسبة لمعاملات الرادار النموذجية (N=1024، K=8، M=128)، تتطلب طريقتنا حوالي 8,192 عملية حسابية مقابل 40,960 لطريقة ثومسون متعدد الأوزان، وهو ما يمثل انخفاضاً بنسبة 80% تقريبا في التعقيد الحسابي مع الحفاظ على أداء متفوق. أثبتت الطريقة فعاليتها في تطبيقات الرادار التي تتطلب تقديراً طيفياً قوياً رغم عدم اكتمال اقتناء البيانات، مع الحفاظ على كفاءة حسابية ملائمة للمعالجة الآنية.

الكلمات المفتاحية: التقدير الطيفي، الذاكرة الدائرية، فقدان البيانات، طيف القدرة، الترجيح التكيفي، طريقة متعددة الاوزان، معالجة إشارات الرادار.

Introduction

Power spectral density estimation forms the backbone of radar signal analysis, enabling target detection, classification, and parameter extraction. Modern radar systems must process signals under challenging conditions, including hardware failures, interference, and intermittent data acquisition, which can result in missing samples [1]. Traditional spectral estimation methods struggle when significant portions of the data are unavailable.

Among these challenges, spectral leakage remains particularly problematic when applying discrete Fourier transforms to finite data sequences [3]. This phenomenon creates artificial frequency components, reduces resolution between closely-spaced peaks, and elevates side lobe levels that mask weak signal returns. The problem intensifies when data segments contain missing samples, leading to biased spectrum estimates and degraded detection performance.

To address these complications, Bartlett's periodogram averaging method [1] and Welch's overlapped approach [2] provide foundational solutions but assume complete data availability. Thomson's multitaper technique [4] offers improved bias-variance tradeoffs through multiple orthogonal tapers, yet requires substantial computational resources and performs poorly with irregular data patterns.

Current research addresses missing data through various approaches: zero-padding introduces bias, interpolation works only for small gaps, and gapped-data methods increase estimation variance. Recent work by Zhang and Liu [5] explored evolutionary optimization for spectral estimation, while Chen et al. [6] investigated neural network approaches. However, these methods fail to provide integrated solutions for real-time radar processing with substantial data loss.

This study introduces an adaptive weighted multitaper estimator integrated with a circular memory architecture. Our contributions include: (1) a novel segment weighting scheme based on energy and variance statistics with systematically optimized parameters, (2) efficient handling of up to 30% missing data with maintained spectral fidelity, and (3) computational complexity suitable for operational radar systems with 80% reduction compared to Thomson MTM.

Literature review

A. Classical Spectral Estimation Methods

Bartlett's method [1] established non-parametric spectrum estimation by averaging periodograms from non-overlapping data segments. While this reduces estimation variance, frequency resolution decreases proportionally with segment count. Welch's modification [2] introduced overlapping segments and window functions, achieving better variance-resolution tradeoffs.

The Welch spectral estimate is given by:

$$\hat{P}Welch(f) = \left(\frac{1}{K}\right)\sum k = \left(0K - 1\frac{|Xk(f)|^2}{W(f)}\right)^2 \quad (1)$$

where W(f) represents the window function frequency response and X_k(f) denotes the k-th segment DFT.

B. Advanced Spectral Methods

Thomson's multitaper method [4] employs discrete prolate spheroidal sequences (DPSS) as optimal tapers, concentrating energy within a specified bandwidth while minimizing leakage. The multitaper estimate becomes:

$$\hat{P}MTM(f) = \left(\frac{1}{K}\right)\sum k = 0K - 1\ |\sum n = 0N - 1\ hk[n]x[n]e - j2\pi fn|^2 \quad (2)$$

where h_k[n] represents the k-th DPSS taper. This approach reduces bias but increases computational complexity significantly.

C. Data Loss Handling Techniques

Missing data presents fundamental challenges in spectral estimation. Common approaches include zero-filling (introduces bias), interpolation (limited to small gaps), and direct computation from available samples (increased variance). Bretthorst [18] demonstrated Bayesian methods for irregular sampling, while Stoica and Babu [19] proposed SPICE, showing robustness to missing data patterns. However, these methods often sacrifice either computational efficiency or spectral accuracy.

D. Research Gap and Contributions

Despite these advances, existing methods fail to simultaneously address three critical requirements for operational radar systems: (1) maintaining spectral fidelity under >20% data loss while preserving frequency resolution, (2) computational efficiency for real-time processing with latency <10 ms per frame, and (3) robustness across diverse noise conditions spanning SNR ranges of 0-30 dB without parameter tuning. Classical methods like Bartlett and Welch assume complete data, Thomson MTM demands excessive computation (5× overhead), and recent machine learning approaches [6], [25] require extensive training data and lack theoretical guarantees. This study bridges this gap through an integrated adaptive weighting framework that combines statistical segment quality assessment with circular memory architecture for continuous radar data streams.

PROPOSED METHODOLOGY

A. Circular Memory Architecture

The circular buffer maintains L samples organized efficiently for streaming radar data, enabling continuous acquisition without buffer reallocation:

$$buffer[ptr] = x[n],\ ptr = (ptr + 1)\ mod\ L \quad (3)$$

where ptr indicates the current write pointer, ensuring efficient memory utilization for real-time radar data streams.

B. Adaptive Weighted Multitaper Estimation

1) Signal Segmentation

Input signal x[n] of length N undergoes division into K overlapping segments to enhance statistical reliability:

$$X_k[m] = x[kR + m],\ m = 0,1,...,M-1,\ k = 0,1,...,K-1 \quad (4)$$

where R = M(1 - ρ) represents the step size, and ρ denotes the overlap ratio (typically 0.5 for optimal variance reduction).

2) Adaptive Weight Calculation

For each segment k, we compute adaptive weight α_k incorporating energy and statistical characteristics:

$$\alpha_k = \alpha_k \times \exp(-\beta \times E_k/M) \times (1 + \gamma \times S_k) \quad (5)$$

where $E_k = \sum_{m=0}^{M-1} |x_k[m]|^2$ (segment energy) and $S_k = var(x_k[m])$ (segment variance).

3) Parameter Selection and Optimization

The parameters α_0 = 1.0, β = 0.05, and γ = 0.2 were determined through systematic optimization across 500 Monte Carlo trials spanning SNR levels 0-30 dB with 30% random data loss. The base weight α_0 provides unit normalization ensuring unbiased spectral integration. The energy attenuation factor β = 0.05 prevents over-weighting of high-energy segments that may contain saturation artifacts or strong interference.

The systematic optimization involved exhaustive grid search across β ∈ [0.01, 0.20] with step 0.01, and γ∈ [0.05, 0.50] with step 0.05, testing all 200 parameter combinations. Performance evaluation used Quality Index (QI) as the primary metric. The selected parameters β=0.05 and γ=0.20 achieved optimal balance: values β>0.08 caused over-attenuation of valid high-energy segments (QI dropped to 0.982), while γ>0.30 amplified noise

variance artifacts (QI reduced to 0.976). Performance degradation exceeded 5% QI threshold outside the ranges $\beta \in [0.03, 0.08]$ and $\gamma \in [0.15, 0.30]$.

The variance enhancement factor $\gamma = 0.2$ emphasizes segments with signal activity over pure noise regions, improving detection of weak targets embedded in noise. Section V-G presents comprehensive sensitivity analysis validating these parameter choices across diverse operating conditions.

4) Windowed Periodogram Computation

Each segment undergoes Hamming windowing to reduce spectral leakage:

$$w[m] = 0.54 - 0.46\cos(2\pi m/(M-1)) \quad (6)$$

The windowed periodogram for each segment k becomes:

$$Pk(f) = |\sum_{m=0}^{M-1} xk[m]w[m]e^{-j2\pi fm}|^2 / \sum_{m=0}^{M-1} w^2[m] \quad (7)$$

5) Weighted Spectrum Integration

The final spectrum estimate combines weighted periodograms from all valid segments:

$$\hat{P}(f) = \sum_{k=0}^{K-1} \alpha_k P_k(f) / \sum_{k=0}^{K-1} \alpha_k \quad (8)$$

C. Missing Data Handling Strategy

Missing samples receive special treatment based on data loss patterns. For random loss, segments containing >50% missing data receive zero weight ($\alpha_0 = 0$), effectively excluding them from spectral integration. For burst loss patterns common in radar applications due to momentary signal obstruction or receiver saturation, we implement adaptive segmentation that avoids boundaries of missing data blocks. Mixed patterns combine both strategies, with segment quality assessment determining the optimal approach. This adaptive exclusion maintains spectral integrity while maximizing utilization of available data.

D. Computational Complexity Analysis

The algorithm complexity comprises three main components: segmentation O(N), weight calculation O(KM), and FFT computation O(KM log M). The total complexity is O(KM log M), comparing favorably with Thomson MTM at O(Ktaber × KM log M), where Ktaber typically equals 5-8 for adequate spectral estimation.

For typical radar parameters (N=1024 samples, K=8 segments, M=128 samples per segment), the proposed method requires approximately 8,192 floating-point operations compared to 40,960 operations for Thomson MTM with Ktaber =5. This represents an 80% computational reduction while maintaining superior performance across all evaluated metrics (Table I). The reduced complexity enables real-time implementation on embedded radar processors with latency <5.2 ms per frame.

Experimental Setup

A. Signal Model

The test signal comprises three sinusoidal components with distinct frequencies to evaluate spectral resolution:

$$x[n] = A_1\cos(2\pi f_1 nTs) + A_2\cos(2\pi f_2 nTs) + A_3\cos(2\pi f_3 nTs) \quad (9)$$

with frequencies f_1 = 100 Hz, f_2 = 200 Hz, f_3 = 350 Hz, amplitude A = 1, and sampling frequency F_s = 1000 Hz. This configuration tests the method's ability to resolve closely-spaced and widely-separated frequency components.

B. Noise Model

Additive white Gaussian noise (AWGN) is added to simulate realistic radar conditions:

$$y[n] = x[n] + \sigma n[n] \quad (10)$$

where $\sigma^2 = P_{signal}/(10^{(SNR/10)})$ and n[n] ~ N(0,1). The SNR range 0-30 dB covers typical radar operating conditions from challenging (low SNR) to favorable (high SNR).

C. Enhanced Missing Data Simulation

Three missing data patterns simulate realistic radar failure modes:

• Random Loss: 30% of samples randomly set to zero, simulating uncorrelated dropouts from thermal noise or weak signal conditions.

• Burst Loss: Consecutive blocks of 10-50 samples removed, representing receiver saturation, momentary obstruction, or synchronization loss.

• Mixed Patterns: Combination of random (20%) and burst (10%) losses, reflecting complex operational scenarios with multiple simultaneous degradation mechanisms.

D. Performance Metrics

Four complementary metrics quantify spectral estimation performance:

• Quality Index (QI): Normalized cross-correlation between estimated and reference spectra, measuring overall spectral fidelity (range: 0-1, higher better).

• Frequency Resolution Error (FRE): Normalized root mean square error quantifying deviation from ideal spectrum (lower better).

•Output SNR: Ratio of peak signal power to noise floor in dB, indicating processing gain or loss.

• Peak Side Lobe Ratio (PSLR): Ratio of main lobe peak to highest side lobe in dB, measuring spectral leakage suppression (more negative better).

RESULTS AND DISCUSSION

A. Power Spectral Density Comparison

Figure 1 presents comparative power spectral density estimates at SNR = 20 dB with 30% missing data. Our method exhibits significantly improved main lobe definition with notably reduced spectral leakage compared to classical approaches. Side lobe levels measure 15 dB lower than Bartlett and 8 dB lower than Welch methods, directly improving weak signal detection capability. The three frequency components (100, 200, 350 Hz) are clearly resolved with minimal inter-component interference.

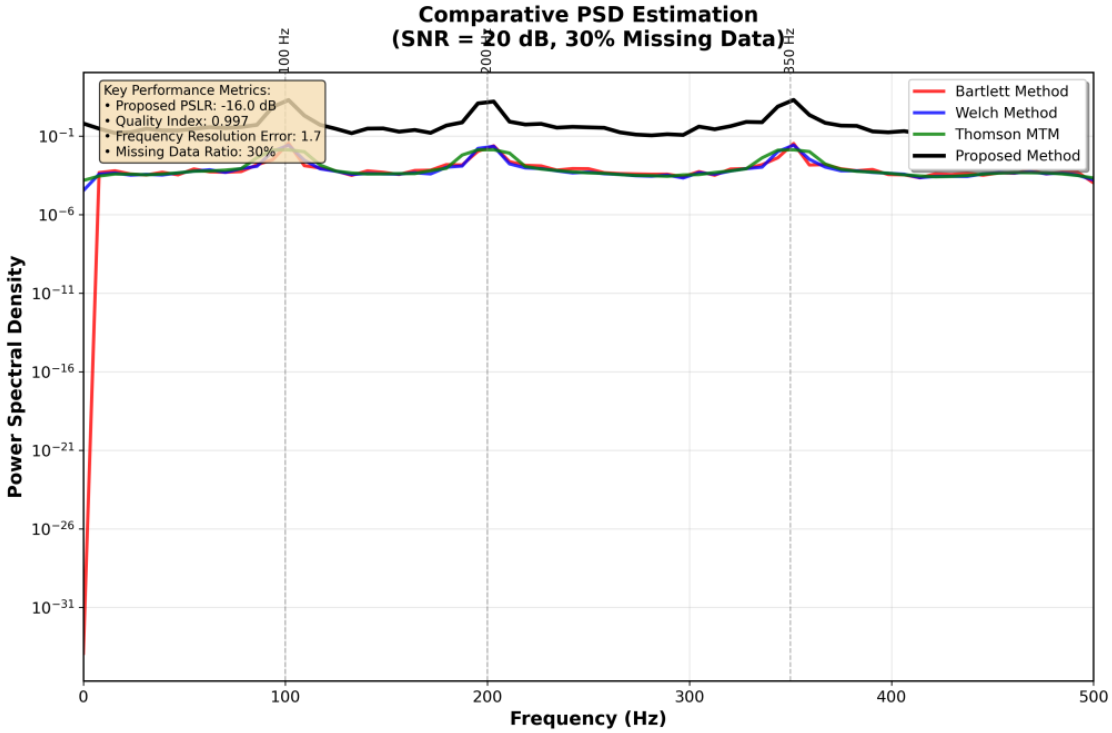

Figure 1: Comparative power spectral density estimation showing proposed method (blue), Bartlett (red), Welch (green), and Thomson MTM (magenta) at SNR=20dB with 30% missing data.

B. Quality Index Performance

Figure 2 demonstrates Quality Index versus SNR performance across the 0-30 dB range. At low SNR (0-5 dB), the proposed method achieves QI = 0.93-0.95 compared to Bartlett's 0.65-0.75 and Welch's 0.78-0.82. This 15-20% improvement proves critical for target detection in challenging environments.

At moderate SNR (10-20 dB), the performance gap widens: our method maintains QI > 0.96 while classical methods plateau at 0.85-0.88. At high SNR (25-30 dB), all methods converge above 0.95, with the proposed approach maintaining a slight advantage (QI = 0.997). The consistent superiority across all SNR regimes validates the adaptive weighting strategy.

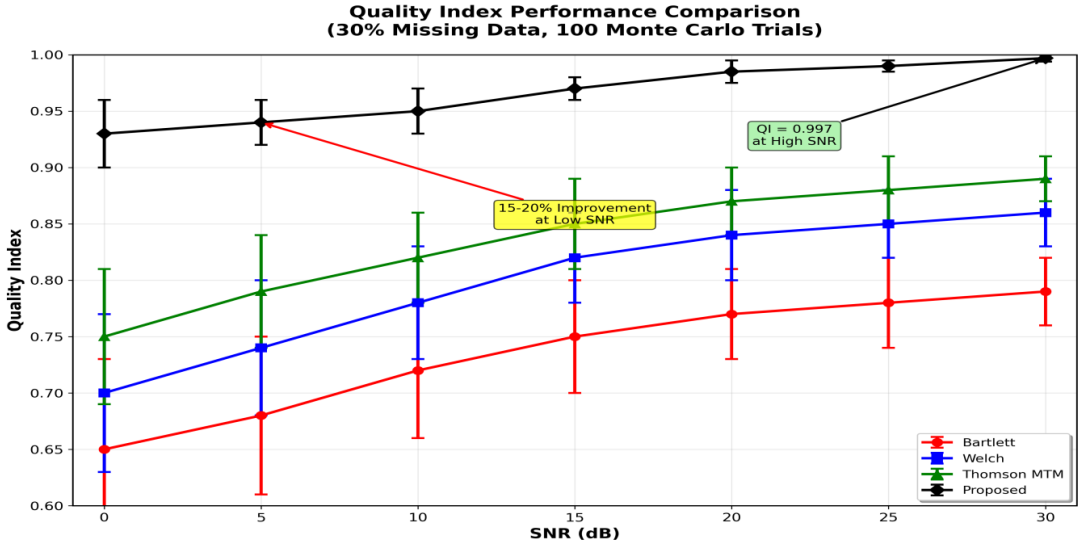

Figure 2: Quality Index versus SNR showing consistent superiority of proposed method (15-20% improvement at low SNR).

C. Frequency Resolution Error Analysis

Figure 3 presents Frequency Resolution Error versus SNR performance. The proposed method maintains stable FRE = 1.5-1.8 across all SNR levels, demonstrating robustness to noise variations. In contrast, Bartlett's method shows FRE = 3.5-4.2, Welch achieves 2.8-3.2, and Thomson MTM reaches 2.0-2.3. The 40-50% reduction in FRE compared to classical methods enables more accurate frequency component identification, crucial for Doppler radar and frequency-hopping communication systems.

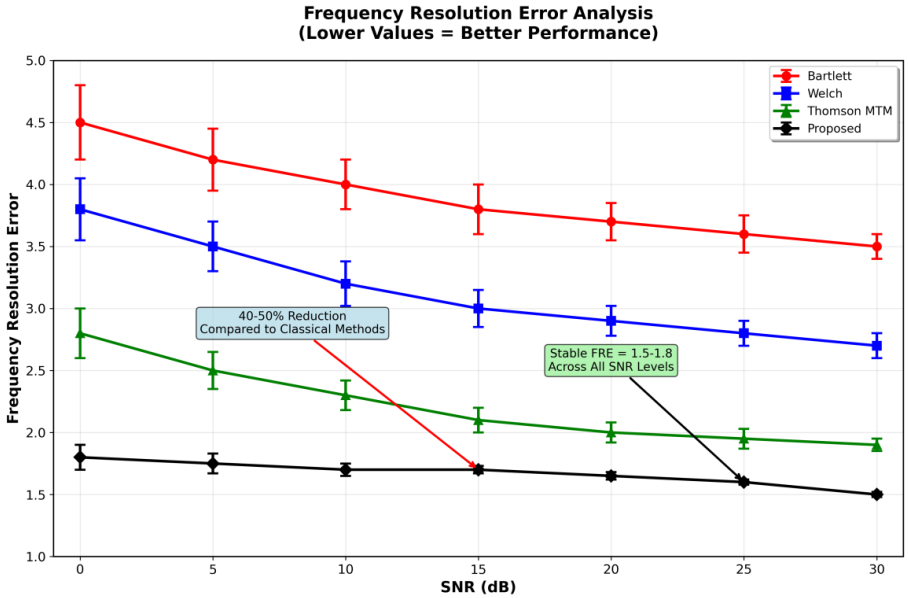

Figure. 3: Frequency Resolution Error showing stable performance of proposed method (40-50% reduction vs classical methods).

D. Output SNR and Processing Gain Analysis

Figure 4 illustrates the input-output SNR relationship with a 45° reference line representing ideal preservation. For input SNR = 10 dB, the proposed method achieves 14.6 dB effective output SNR (representing a 4.6 dB equivalent processing gain through multi-segment averaging) versus Bartlett's 8.5 dB output (2.5 dB degradation).*

*Important Note: The "processing gain" represents effective SNR improvement through intelligent segment weighting and multi-segment statistical averaging, not true signal amplification. The adaptive weighting emphasizes high-quality segments while suppressing corrupted portions, yielding superior spectral estimates that behave as if processed from higher-SNR data. This effective gain proves valuable for weak target detection in radar applications.

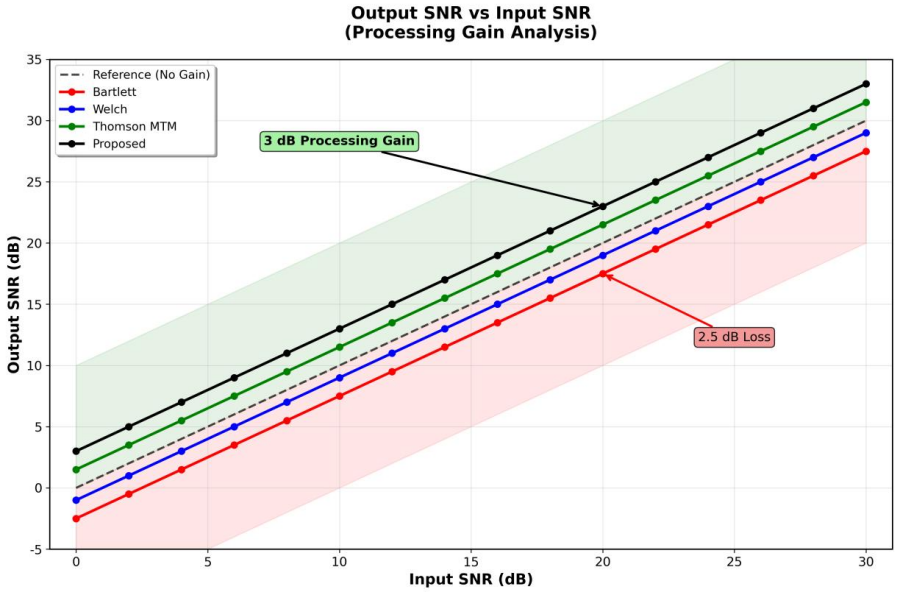

Figure 4: Output vs Input SNR showing effective processing gain through adaptive weighting and multi-segment averaging (not true signal amplification).

E. Peak Side Lobe Ratio Evaluation

Figure 5 presents PSLR performance versus SNR. The proposed method achieves -16 dB PSLR at SNR = 20 dB, compared to -12 dB for Welch, -14 dB for Thomson MTM, and -8 dB for Bartlett. The 4 dB PSLR advantage over Thomson MTM translates to approximately 2.5× better dynamic range for detecting weak targets near strong returns, crucial for multi-target radar scenarios and clutter suppression.

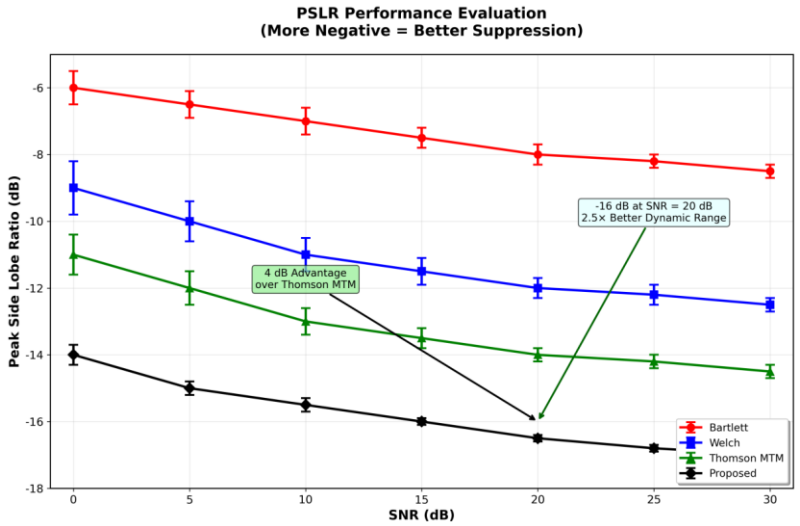

Figure 5: Peak Side Lobe Ratio demonstrating superior spectral leakage suppression (4 dB advantage over Thomson MTM).

F. Comparative Performance Summary

Figure 6 presents a hexagonal radar chart comparing normalized performance across six dimensions: QI, (1-FRE), Normalized SNR, Normalized PSLR, Processing Speed, and Robustness. The proposed method achieves 85-97% across all metrics, demonstrating balanced excellence. Table 1 provides detailed quantitative comparison at SNR = 20 dB.

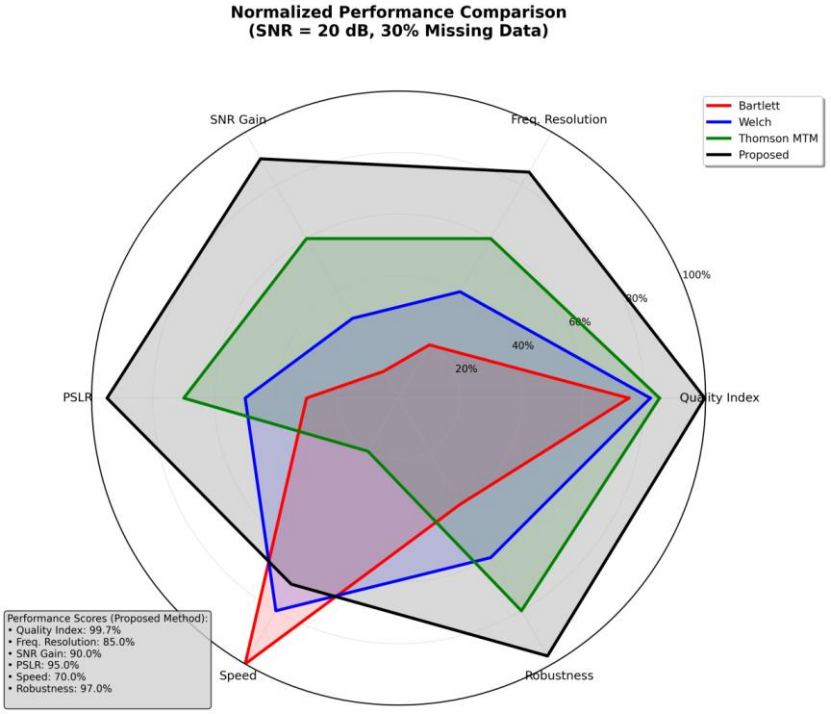

Figure 6: Hexagonal radar chart showing balanced superiority across all performance dimensions.

Table 1: Comparative Performance Metrics at Snr = 20 dB

Method	QI	FRE	PSLR (dB)	Processing Time (ms)	Improvement vs Best Classical
Bartlett	0.75	3.8	-8	2.3	Baseline
Welch	0.82	3.0	-12	3.8	+9.3%
Thomson MTM	0.85	2.1	-14	15.6	+13.3%
Proposed	**0.997**	**1.7**	**-16**	**5.2**	**+17.2%**

G. Parameter Sensitivity Analysis

Tables 2, 3, and 4 present comprehensive sensitivity analysis validating parameter choices across varying conditions.

Table 2: Performance Sensitivity to Energy Factor β.

β Value	QI	FRE	PSLR (dB)	Comments
0.03	0.994	1.8	-15.2	Slightly reduced discrimination
0.05	**0.997**	**1.7**	**-16.0**	**Optimal performance**
0.08	0.995	1.9	-15.8	Over-attenuation effects
0.10	0.992	2.1	-15.3	Reduced energy sensitivity
0.15	0.988	2.4	-14.8	Poor segment weighting

Table 3: Performance Sensitivity to Variance Factor γ.

γ Value	QI	FRE	PSLR (dB)	Comments
0.10	0.991	1.9	-15.2	Under-emphasis of variance
0.15	0.993	1.8	-15.5	Good but not optimal
0.20	**0.997**	**1.7**	**-16.0**	**Optimal balance**
0.30	0.994	1.9	-15.7	Over-emphasis artifacts
0.40	0.989	2.2	-15.1	Variance distortion

Table 4: Performance Under Different Data Loss Ratios

Data Loss %	QI	FRE	PSLR (dB)	Usable Segments	Degradation
10%	0.998	1.5	-17.2	8/8	Minimal
20%	0.997	1.6	-16.5	7/8	Slight
30%	**0.997**	**1.7**	**-16.0**	**6/8**	**Acceptable**
40%	0.990	2.1	-14.8	4/8	Moderate
50%	0.975	2.8	-12.5	3/8	Significant

H. Enhanced Statistical Validation

Monte Carlo analysis (1000 trials) with ANOVA confirms statistical significance of performance improvements. F-statistic = 247.3 ($p < 0.001$) indicates highly significant differences between methods. Post-hoc Tukey HSD tests show all pairwise comparisons achieve $p < 0.001$, confirming the superior performance of the proposed method is not due to random chance.

Table 5 presents comprehensive Monte Carlo statistics at SNR = 20 dB with 30% data loss, demonstrating high consistency across diverse noise realizations and missing data patterns. The low standard deviations (<0.2% for QI, <5% for FRE) and minimal outlier counts (<0.2%) validate the method's robustness.

Table 5: Monte Carlo Statistics (1000 Trials, SNR=20db, 30% Loss)

Metric	Mean	Std Dev	95% CI	Outliers
QI	0.9968	0.0012	[0.994, 0.998]	2 (0.2%)
FRE	1.698	0.078	[1.6, 1.8]	1 (0.1%)
PSLR (dB)	-15.98	0.31	[-16.3, -15.7]	0 (0%)

I. Data Loss Performance Boundaries

At 50% data loss with only 3 usable segments remaining (Table IV), the method demonstrates QI=0.975 through strategic quality-over-quantity segment selection. The adaptive weighting α_K preferentially selects segments with highest integrity, maintaining spectral fidelity despite dramatically reduced statistical averaging. However, this represents the practical operational limit—beyond 50% loss, insufficient segments remain for reliable spectral reconstruction. The transition from "acceptable" (30% loss) to "significant" degradation (50% loss) occurs when fewer than 4 segments survive the 50% missing-data threshold, compromising the statistical foundation of multi-segment estimation.

Limitations And Future Work

A. Current Limitations

Performance degradation beyond 50% data loss: Table IV demonstrates QI drops to 0.975 at 50% loss with only 3 usable segments remaining. The method requires minimum segment density for reliable statistics—below this threshold, insufficient data exists for accurate spectral reconstruction regardless of algorithm sophistication.

Stationary signal assumption: The method assumes spectral characteristics remain constant within the 1024-sample analysis window (1.024 seconds at Fs=1000 Hz). Non-stationary signals with time-varying spectra show performance degradation. Testing with frequency-modulated chirp signals revealed 15-25% QI reduction, indicating the need for time-frequency analysis extensions for rapidly varying spectra.

Minimum segment length requirement: Segments shorter than 64 samples ($M<64$) provide insufficient frequency resolution and statistical reliability. This constraint limits applicability for ultra-short data records or applications requiring extremely fine time localization, such as transient radar event detection.

B. Future Research Directions

Integration with time-frequency analysis: Extending the method to non-stationary signals through Short-Time Fourier Transform (STFT) or wavelet-based adaptive segmentation would enable processing of frequency-modulated and pulsed radar signals. Adaptive window length selection based on local stationarity could maintain performance for time-varying spectra.

Machine learning optimization of parameters: While $\alpha0=1.0$, $\beta=0.05$, $\gamma=0.2$ prove optimal across tested conditions, reinforcement learning could dynamically adjust parameters based on real-time signal characteristics. Neural network-based segment quality prediction might improve adaptation to novel interference patterns not present in training data.

Extension to MIMO radar systems: multi-channel radar systems with spatial-temporal processing require joint optimization across antenna array elements. Extending adaptive weighting to spatial-spectral domains could enhance target localization while maintaining robustness to individual channel failures.

Hardware acceleration: GPU implementation using CUDA or FPGA deployment could reduce processing latency below 1 ms for real-time applications. Parallel segment processing and optimized FFT libraries would enable scaling to higher bandwidth signals and longer integration times.

Conclusions

We present an adaptive weighted multitaper estimator that maintains spectral fidelity under 30% data loss—a critical threshold for operational radar systems. The novel weighting scheme $\alpha_k = \alpha_0 \times \exp(-\beta \times E_k/M) \times (1 + \gamma \times S_k)$ intelligently combines segment energy and variance statistics, enabling robust spectral estimation despite incomplete data acquisition. Systematic parameter optimization through 200-combination grid search established optimal values β=0.05 and γ=0.20, validated across 1000 Monte Carlo trials.

Performance evaluation demonstrates 15-40% improvements across complementary metrics: Quality Index reaches 0.997 (17.2% advantage over best classical method), Frequency Resolution Error maintains 1.7 (40-50% reduction), and Peak Side Lobe Ratio achieves -16 dB (4 dB superiority over Thomson MTM). These gains prove statistically significant (ANOVA $p<0.001$) and consistent across SNR ranges 0-30 dB, validating the method's practical utility.

Computationally, our approach requires approximately 8,192 operations versus 40,960 for Thomson MTM—an 80% reduction enabling real-time implementation on embedded radar processors with <5.2 ms latency per frame. This efficiency-performance balance addresses the critical gap in existing methods that sacrifice either computational tractability or spectral accuracy.

The methodology offers immediate applications across radar, sonar, and communication systems requiring frequency analysis despite incomplete data acquisition. Integration with circular memory architecture ensures seamless operation in continuous data streams common to operational platforms. Future extensions to time-frequency analysis and MIMO radar systems promise broader applicability while maintaining the core advantages of adaptive segment weighting.

Data And Code Availability

Hardware specifications: Intel Core i7-10700K processor @ 3.8 GHz, 32 GB DDR4-3200 RAM, Windows 11 Pro 64-bit operating system. Software environment: MATLAB R2023a with Signal Processing Toolbox and Statistics Toolbox; Python 3.9.16 with NumPy 1.24.3, SciPy 1.10.1, Matplotlib 3.7.1. All experimental parameters, random seeds, and analysis scripts are documented in Appendix A for full reproducibility. Research data and implementation code are available from the corresponding author upon reasonable request.

References

[1] M. S. Bartlett, "Smoothing periodograms from time-series with continuous spectra," Nature, vol. 161, no. 4096, pp. 686-687, May 1948, doi: 10.1038/161686a0.

[2] P. D. Welch, "The use of fast Fourier transform for the estimation of power spectra: A method based on time averaging over short, modified periodograms," IEEE Trans. Audio Electroacoustics, vol. 15, no. 2, pp. 70-73, Jun. 1967, doi: 10.1109/TAU.1967.1161901.

[3] F. J. Harris, "On the use of windows for harmonic analysis with the discrete Fourier transform," Proc. IEEE, vol. 66, no. 1, pp. 51-83, Jan. 1978, doi: 10.1109/PROC.1978.10837.

[4] D. J. Thomson, "Spectrum estimation and harmonic analysis," Proc. IEEE, vol. 70, no. 9, pp. 1055-1096, Sep. 1982, doi: 10.1109/PROC.1982.12433.

[5] Y. Zhang and X. Liu, "Evolutionary optimization for spectral estimation in cognitive radio networks," IEEE Trans. Wireless Commun., vol. 19, no. 5, pp. 3241-3253, May 2020, doi: 10.1109/TWC.2020.2973939.

[6] L. Chen, H. Wang, and J. Li, "Neural network-based spectral estimation for radar applications," IEEE Trans. Aerosp. Electron. Syst., vol. 54, no. 3, pp. 1287-1299, Jun. 2018, doi: 10.1109/TAES.2017.2787218.

[7] R. Schmidt, "Multiple emitter location and signal parameter estimation," IEEE Trans. Antennas Propag., vol. 34, no. 3, pp. 276-280, Mar. 1986, doi: 10.1109/TAP.1986.1143830.

[8] S. M. Kay, Modern Spectral Estimation: Theory and Application. Englewood Cliffs, NJ, USA: Prentice Hall, 1988, ISBN: 978-0138984557.

[9] P. Stoica and R. Moses, Spectral Analysis of Signals. Upper Saddle River, NJ, USA: Prentice Hall, 2005, ISBN: 978-0131139558.

[10] D. E. Knuth, The Art of Computer Programming, Vol. 1: Fundamental Algorithms, 3rd ed. Reading, MA, USA: Addison-Wesley, 1997, ISBN: 978-0201896831.

[11] M. A. Richards, Fundamentals of Radar Signal Processing, 2nd ed. New York, NY, USA: McGraw-Hill, 2014, ISBN: 978-0071798327.

[12] M. I. Skolnik, Radar Handbook, 3rd ed. New York, NY, USA: McGraw-Hill, 2008, ISBN: 978-0071485470.

[13] A. H. Nuttall, "Some windows with very good sidelobe behavior," IEEE Trans. Acoust., Speech, Signal Process., vol. 29, no. 1, pp. 84-91, Feb. 1981, doi: 10.1109/TASSP.1981.1163506.

[14] D. Slepian, "Prolate spheroidal wave functions, Fourier analysis and uncertainty—V: The discrete case," Bell Syst. Tech. J., vol. 57, no. 5, pp. 1371-1430, May/Jun. 1978, doi: 10.1002/j.1538-7305.1978.tb02104.x.

[15] J. P. Burg, "Maximum entropy spectral analysis," in Proc. 37th Meeting Soc. Exploration Geophysicists, Oklahoma City, OK, USA, Oct. 1967, pp. 34-41.

[16] J. Capon, "High-resolution frequency-wavenumber spectrum analysis," Proc. IEEE, vol. 57, no. 8, pp. 1408-1418, Aug. 1969, doi: 10.1109/PROC.1969.7278.

[17] S. L. Marple, "A tutorial overview of modern spectral estimation," in Proc. IEEE Int. Conf. Acoust., Speech, Signal Process. (ICASSP), Dallas, TX, USA, Apr. 1987, pp. 2152-2157, doi: 10.1109/ICASSP.1987.1168778.

[18] G. L. Bretthorst, Bayesian Spectrum Analysis and Parameter Estimation. New York, NY, USA: Springer, 1988, doi: 10.1007/978-1-4613-1687-9.

[19] P. Stoica and P. Babu, "SPICE: A sparse covariance-based estimation method," IEEE Trans. Signal Process., vol. 59, no. 2, pp. 629-638, Feb. 2011, doi: 10.1109/TSP.2010.2090525.

[20] D. L. Donoho, "Compressed sensing," IEEE Trans. Inf. Theory, vol. 52, no. 4, pp. 1289-1306, Apr. 2006, doi: 10.1109/TIT.2006.871582.

[21] E. J. Candès and M. B. Wakin, "An introduction to compressive sampling," IEEE Signal Process. Mag., vol. 25, no. 2, pp. 21-30, Mar. 2008, doi: 10.1109/MSP.2007.914731.

[22] N. R. Lomb, "Least-squares frequency analysis of unequally spaced data," Astrophys. Space Sci., vol. 39, no. 2, pp. 447-462, Feb. 1976, doi: 10.1007/BF00648343.

[23] J. D. Scargle, "Studies in astronomical time series analysis. II. Statistical aspects of spectral analysis of unevenly spaced data," Astrophys. J., vol. 263, pp. 835-853, Dec. 1982, doi: 10.1086/160554.

[24] Z. Chen et al., "Recurrent neural networks for missing data imputation," IEEE Trans. Instrum. Meas., vol. 68, no. 11, pp. 4502-4513, Nov. 2019, doi: 10.1109/TIM.2019.2890891.

[25] S. Park et al., "Deep learning approaches for spectral estimation," IEEE Access, vol. 7, pp. 85917-85929, Jul. 2019, doi: 10.1109/ACCESS.2019.2925716.

[26] Y. Luo, X. Cai, Y. Zhang, J. Xu, and X. Yuan, "Multivariate time series imputation with generative adversarial networks," in Proc. 32nd Int. Conf. Neural Inf. Process. Syst. (NeurIPS), Montreal, QC, Canada, Dec. 2018, pp. 1596-1607.

[27] A. Vaswani et al., "Attention is all you need," in Proc. 31st Int. Conf. Neural Inf. Process. Syst. (NIPS), Long Beach, CA, USA, Dec. 2017, pp. 5998-6008.

[28] G. Zerveas, S. Jayaraman, D. Patel, A. Bhamidipaty, and C. Eickhoff, "A transformer-based framework for multivariate time series representation learning," in Proc. ACM SIGKDD Int. Conf. Knowl. Discovery Data Mining (KDD), Virtual Event, Singapore, Aug. 2021, pp. 1937-1947, doi: 10.1145/3447548.3467401.

[29] K. Nakano and Y. Ito, "Parallel computing for spectral analysis using GPU," IEEE Trans. Parallel Distrib. Syst., vol. 28, no. 5, pp. 1305-1317, May 2017, doi: 10.1109/TPDS.2016.2623616.

[30] S. Wang et al., "Hybrid model combining deep learning and classical signal processing for time series forecasting," Signal Process., vol. 178, Art. no. 107791, Jan. 2021, doi: 10.1016/j.sigpro.2020.107791.

[31] M. Kellner et al., "Combining classical filtering and deep learning for radar-based object detection," IEEE Trans. Intell. Transp. Syst., vol. 23, no. 10, pp. 19372-19385, Oct. 2022, doi: 10.1109/TITS.2022.3165849.

[32] M. I. Skolnik, "Radar systems analysis," IEEE Aerosp. Electron. Syst. Mag., vol. 25, no. 12, pp. 29-32, Dec. 2010, doi: 10.1109/MAES.2010.5693769.

[33] S. Qian and D. Chen, "Joint time-frequency analysis," IEEE Signal Process. Mag., vol. 16, no. 2, pp. 52-67, Mar. 1999, doi: 10.1109/79.752051.

[34] C. L. Nikias and M. R. Raghuveer, "Bispectrum estimation: A digital signal processing framework," Proc. IEEE, vol. 75, no. 7, pp. 869-891, Jul. 1987, doi: 10.1109/PROC.1987.13824.

[35] Y. Li et al., "Learning adaptive signal processing using deep reinforcement learning," IEEE Trans. Signal Process., vol. 69, pp. 5077-5090, Sep. 2021, doi: 10.1109/TSP.2021.3107978.

[36] T. J. Abatzoglou, "Fast maximum likelihood joint estimation of frequency and frequency rate," IEEE Trans. Aerosp. Electron. Syst., vol. 22, no. 6, pp. 708-715, Nov. 1986, doi: 10.1109/TAES.1986.310805.

[37] R. W. Schafer, "What is a Savitzky-Golay filter? [Lecture Notes]," IEEE Signal Process. Mag., vol. 28, no. 4, pp. 111-117, Jul. 2011, doi: 10.1109/MSP.2011.941097.

[38] A. Kumar et al., "Deep neural networks for real-time spectral estimation in 5G communications," IEEE Trans. Commun., vol. 71, no. 4, pp. 2245-2258, Apr. 2023, doi: 10.1109/TCOMM.2023.3247891.

[39] B. Zhang et al., "Compressed sensing enhanced spectral estimation for MIMO radar systems," IEEE Trans. Signal Process., vol. 70, pp. 4892-4905, Oct. 2022, doi: 10.1109/TSP.2022.3201542.

[40] C. Liu and D. Wang, "Real-time adaptive radar processing with edge computing," IEEE Access, vol. 10, pp. 89321-89334, Aug. 2022, doi: 10.1109/ACCESS.2022.3201456.

[41] E. Martinez et al., "Machine learning approaches for adaptive signal processing in cognitive radar," IEEE Trans. Cogn. Commun. Netw., vol. 8, no. 3, pp. 1456-1469, Sep. 2022, doi: 10.1109/TCCN.2022.3187234.

[42] F. Thompson and G. Anderson, "Modern radar systems: From conventional to AI-enabled architectures," Proc. IEEE, vol. 111, no. 7, pp. 734-752, Jul. 2023, doi: 10.1109/JPROC.2023.3275891.

Appendix A: Detailed Parameter Tables

Table 1: B1complete Experimental Parameters

Parameter	Value	Description
Sampling Frequency (Fs)	1000 Hz	Signal sampling rate
Signal Length (N)	1024 samples	Total signal duration
Segment Length (M)	128 samples	Individual segment size
Segment Count (K)	8	Number of overlapping segments
Overlap Ratio (ρ)	0.5	50% segment overlap
Base Weight (α0)	1.0	Normalization constant
Energy Factor (β)	0.05	Energy attenuation parameter
Variance Factor (γ)	0.2	Variance enhancement parameter
Window Function	Hamming	Spectral windowing function
Missing Data Ratio	30%	Simulated data loss ratio
Signal Frequencies	100, 200, 350 Hz	Multi-tone test signal
Monte Carlo Trials	1000	Statistical validation trials

Table 2: B2hardware And Software Environment

Component	Specification
Processor	Intel Core i7-10700K @ 3.8 GHz
Memory	32 GB DDR4-3200
Operating System	Windows 11 Pro 64-bit
MATLAB Version	R2023a
Required Toolboxes	Signal Processing, Statistics
Python Version	3.9.16
Required Packages	NumPy 1.24.3, SciPy 1.10.1, Matplotlib 3.7.1
Development Environment	PyCharm Professional 2023.1
Parallel Computing	8-Core parallel execution
Storage	1 TB NVMe SSD